HAL open science

# Cloud microphysics and aerosol indirect effects in the global climate model ECHAM5-HAM

U. Lohmann, P. Stier, C. Hoose, S. Ferrachat, E. Roeckner, J. Zhang

**To cite this version:**

U. Lohmann, P. Stier, C. Hoose, S. Ferrachat, E. Roeckner, et al.. Cloud microphysics and aerosol indirect effects in the global climate model ECHAM5-HAM. Atmospheric Chemistry and Physics Discussions, 2007, 7 (2), pp.3719-3761. ⟨hal-00302651⟩

**HAL Id: hal-00302651**

**https://hal.science/hal-00302651v1**

Submitted on 18 Jun 2008

**HAL** is a multi-disciplinary open access archive for the deposit and dissemination of scientific research documents, whether they are published or not. The documents may come from teaching and research institutions in France or abroad, or from public or private research centers.

L'archive ouverte pluridisciplinaire **HAL**, est destinée au dépôt et à la diffusion de documents scientifiques de niveau recherche, publiés ou non, émanant des établissements d'enseignement et de recherche français ou étrangers, des laboratoires publics ou privés.

Autorisation HAL

HAL Authorization

Atmos. Chem. Phys. Discuss., 7, 3719–3761, 2007
www.atmos-chem-phys-discuss.net/7/3719/2007/
© Author(s) 2007. This work is licensed
under a Creative Commons License.

Atmospheric Chemistry and Physics Discussions

# Cloud microphysics and aerosol indirect effects in the global climate model ECHAM5-HAM

**U. Lohmann[1], P. Stier[2], C. Hoose[1], S. Ferrachat[1], E. Roeckner[3], and J. Zhang[4]**

[1]Institute of Atmospheric and Climate Science, ETH Zurich, Switzerland
[2]Department of Environmental Science and Engineering, California Institute of Technology, Pasadena, USA
[3]Max Planck Institute for Meteorology, Hamburg, Germany
[4]Meteorological Service of Canada, Toronto, Canada

Received: 22 February 2007 – Accepted: 8 March 2007 – Published: 12 March 2007

Correspondence to: U. Lohmann (ulrike.lohmann@env.ethz.ch)

## Abstract

The double-moment cloud microphysics scheme from ECHAM4 has been coupled to the size-resolved aerosol scheme ECHAM5-HAM. ECHAM5-HAM predicts the aerosol mass and number concentrations and the aerosol mixing state. This results in a much better agreement with observed vertical profiles of the black carbon and aerosol mass mixing ratios than with the previous version ECHAM4, where only the different aerosol mass mixing ratios were predicted. Also, the simulated liquid, ice and total water content and the cloud droplet and ice crystal number concentrations as a function of temperature in stratiform mixed-phase clouds between 0 and –35°C agree much better with aircraft observations in the ECHAM5 simulations. ECHAM5 performs better because more realistic aerosol concentrations are available for cloud droplet nucleation and because the Bergeron-Findeisen process is parameterized as being more efficient.

The total anthropogenic aerosol effect includes the direct, semi-direct and indirect effects and is defined as the difference in the top-of-the-atmosphere net radiation between present-day and pre-industrial times. It amounts to $-1.8\,\mathrm{W\,m^{-2}}$ in ECHAM5, when a relative humidity dependent cloud cover scheme and present-day aerosol emissions representative for the year 2000 are used. It is larger when either a statistical cloud cover scheme or a different aerosol emission inventory are employed.

## 1 Introduction

Aerosol effects on warm clouds by increasing the cloud droplet number concentration and decreasing cloud droplet size have been considered in climate models for more than a decade (Jones et al., 1994; Boucher and Lohmann, 1995). While the first climate models used sulfate aerosols as a surrogate for all anthropogenic aerosols, lately climate models have started to consider the major global aerosol components, sulfate, particulate organic matter, black carbon, sea salt and mineral dust. However, this has not led to a smaller uncertainty range of the indirect aerosol effect, because consider-



ACPD

7, 3719–3761, 2007

ing different aerosol species also introduces new uncertainties.

Estimates of the global annual mean cloud albedo enhancement due to the more and smaller cloud droplets for a given cloud water content (cloud albedo effect, Twomey, 1977) range between –0.5 to –1.9 W m$^{-2}$ while the prolongation of cloud lifetime due to the reduction in drizzle production of the smaller cloud droplets (the so-called cloud lifetime effect, Albrecht, 1989) ranges between –0.3 and –1.4 W m$^{-2}$ (Lohmann and Feichter, 2005).

The indirect aerosol effects are larger than estimates of the direct and semi-direct effect. In a model intercomparison of nine different global models, the ensemble model average direct aerosol effect under all-sky conditions amounted to –0.22 W m$^{-2}$ in the annual global mean, ranging from +0.04 to –0.41 W m$^{-2}$ (Schulz et al., 2006). The semi-direct effect refers to temperature changes due to absorbing aerosols that can cause evaporation of cloud droplets, as was shown in a large eddy model simulation study that used black carbon concentrations measured during the Indian Ocean Experiment (Ackerman et al., 2000). It ranges from 0.1 to –0.5 W m$^{-2}$ in global simulations (Lohmann and Feichter, 2005).

Aerosols can also affect ice clouds, however, these indirect aerosol effects are even more uncertain. Global climate model studies suggest that if, in addition to mineral dust, hydrophilic black carbon aerosols are assumed to act as ice nuclei at temperatures between 0 and –35°C, then increases in aerosol concentration from pre-industrial to present times may cause a glaciation indirect effect (Lohmann, 2002a). The glaciation effect refers to an increase in ice nuclei that results in a more frequent glaciation of supercooled stratiform clouds and increases the amount of precipitation via the ice phase. This decreases the global mean cloud cover and allows more solar radiation to be absorbed in the atmosphere. Whether or not the glaciation effect can partly offset the warm indirect aerosol effect depends on the competition between the ice nucleating abilities of the natural and anthropogenic freezing nuclei (Lohmann and Diehl, 2006).

Previous estimates of indirect aerosol effects with the global climate model ECHAM4 were conducted by predicting only the mass mixing ratios of the different aerosol

species. The aerosol number concentration was obtained from log-normal distributions for each aerosol compound, assuming an external aerosol mixture. Recently, size-segregated, interactive multi-component aerosol modules are embedded into global models allowing to simulate the mixing state explicitly (see Stier et al., 2005, for a review). However, the coupling between size-segregated, interactive multi-component aerosol modules with double moment cloud microphysics schemes that consider aerosol effects on water and mixed-phase clouds, has just begun. Jacobson (2006) studied the effect of soot inclusions within clouds and precipitation for global climate but did not focus on indirect aerosol effects.

In this paper we investigate the impact of the more physically based aerosol scheme ECHAM5-HAM (Stier et al., 2005), which predicts the aerosol mixing state in addition to the aerosol mass and number concentrations, together with modifications in the cloud microphysics scheme and different aerosol emissions on aerosol and cloud properties in the present-day climate and for estimates of the total anthropogenic aerosol effect. We focus only on those differences between ECHAM4 and ECHAM5 that are related to the different treatment of aerosols and cloud microphysics as a detailed comparison of these model versions is beyond the scope of this paper. The questions to be answered are:

- What is the impact of the revised parameterization of the Bergeron-Findeisen process on the liquid water versus ice distribution in mixed-phase clouds?
- What is the impact of different biomass burning emissions on the total anthropogenic aerosol effect?
- What is the impact of the cloud cover scheme on the total anthropogenic aerosol effect?

## 2 Model description and set-up of the simulations

We use the new version of the Hamburg general circulation model (GCM) ECHAM5 (Roeckner et al., 2003). As compared to the standard ECHAM4 (Roeckner et al., 1996), it now includes operationally prognostic equations for the mass mixing ratios of cloud liquid water and ice (Lohmann and Roeckner, 1996). For the simulations discussed here, additional prognostic equations of the number concentrations of cloud droplets and ice crystals following their implementation in sensitivity studies with ECHAM4 (Lohmann et al., 1999; Lohmann, 2002b; Lohmann and Diehl, 2006) have also been introduced. ECHAM5 includes a new radiation scheme with 16 bands in the longwave regime (Mlawer et al., 1997). The shortwave code is essentially unchanged except that the number of spectral intervals is 4 instead of 2 in ECHAM4. However, in this study a 6-band version of the code has been applied with two additional bands in the visible and ultraviolet (Cagnazzo et al., 2006). ECHAM5 also includes a new mass and shape-preserving advection scheme (Lin and Rood, 1996).

### 2.1 Aerosols

The double-moment modal aerosol microphysics scheme HAM (Stier et al., 2005) is coupled to ECHAM5 (ECHAM5-HAM). It predicts the evolution of an ensemble of microphysically interacting internally- and externally-mixed aerosol populations as well as their size distribution and composition. The size distribution is represented by a superposition of log-normal modes including the major global aerosol compounds sulfate, black carbon, particulate organic matter, sea salt and mineral dust (Stier et al., 2005). With the prognostic treatment of the mixing state it is possible to maintain an external mixture of hydrophobic particles that become aged to the hydrophilic/mixed modes by the condensation of sulfuric acid and the coagulation with hydrophilic modes.

Aerosol activation is parameterized according to Lin and Leaitch (1997):

$$Q_{\mathrm{nucl}} = \max\left[\frac{1}{\Delta t}\left(0.1\left(\frac{N_a w}{w+\alpha N_a}\right)^{1.27} - N_{l,\mathrm{old}}\right), 0\right] \quad (1)$$

where $N_a$=number concentration of the aerosol particles with a radius >0.035 $\mu$m, $w$=vertical velocity, $\Delta t$=time step, $N_{l,\mathrm{old}}$ is the cloud droplet number concentration from the previous timestep and $\alpha$=0.023 cm$^4$ s$^{-1}$. This simplified assumption is justified because aerosol size dominates aerosol activation in the first instance (Dusek et al., 2006). Moreover, all aerosols that have been in the atmosphere longer than a few hours acquire enough soluble material to participate in cloud droplet nucleation (Dusek et al., 2006). The cut-off radius of 0.035 $\mu$m falls in-between the activation radii observed for maritime and continental aerosols by Dusek et al. (2006). In contrast an external aerosol mixture was assumed in ECHAM4. There all accumulation and coarse mode sea salt and dust particles, accumulation size sulfate aerosols and hydrophilic black and organic carbon were available for nucleation.

The updraft velocity $w$ is obtained as the sum of the grid mean vertical velocity and a turbulent contribution expressed in terms of the turbulent kinetic energy (TKE) for stratiform clouds (Lohmann et al., 1999). For stratiform clouds originating from detrainment of convective clouds also a contribution of the convectively available potential energy (CAPE) (Rogers and Yau, 1989) has been added:

$$w = \begin{cases} \overline{w} + 1.33\sqrt{TKE} & \text{stratiform clouds} \\ \overline{w} + \sqrt{CAPE} + 1.33\sqrt{TKE} & \text{convective clouds} \end{cases} \quad (2)$$

The lower bound on the cloud droplet number concentration whenever a cloud is present is set to 40 cm$^{-3}$ in all simulations (ECHAM4, and the ECHAM5 simulations with the double-moment cloud microphysics scheme).

In the standard ECHAM5-HAM simulations the AeroCom B year 2000 emissions from Dentener et al. (2006) are used. In order to reduce the methodological differences between ECHAM5-HAM and the aerosol scheme in ECHAM4, we conduct one

simulation with ECHAM5-HAM in which we use the 1985 emission inventory that was used for the ECHAM4 simulations (simulation ECHAM5-1985). The main difference between the 2000 emission inventory and the 1985 emission inventory is the methodology of obtaining biomass burning emissions. Whereas the black and organic carbon emissions amount to 11.7 and 105 Tg C in the 1985 emission inventory (Lohmann et al., 1999), they only amount to 7.7 and 47.4 Tg C in the 2000 emission inventory (Stier et al., 2005).

### 2.2 Cloud microphysics

The cloud scheme in ECHAM5 that is used for these studies includes the double-moment cloud microphysics scheme for cloud droplets and ice crystals that has been described in Lohmann et al. (1999) and Lohmann (2002b).

In our standard experiment ECHAM5-RH we use the same fractional cloud cover scheme that has been used in ECHAM4. It diagnoses fractional cloud cover from relative humidity once a critical relative humidity is reached (Sundqvist et al., 1989). ECHAM5 has the option to include a prognostic cloud cover scheme (Tompkins, 2002). It is based on a parameterization for the horizontal subgrid-scale variability of water vapor and cloud condensate, which is used to diagnose cloud fraction in the spirit of statistically based cloud cover parameterizations. This scheme considers that processes, such as deep convection, turbulence, and microphysics, directly affect the higher-order moments of the total water distribution, and thus, have an impact on cloud cover. We investigate the impact of the Tompkins cloud cover scheme in simulation ECHAM5-COV.

Heterogeneous freezing in large-scale mixed-phase clouds considers immersion freezing and contact freezing by dust and soot aerosols and includes the size dependent aerosol diffusivity in the collision efficiency as described in Lohmann and Diehl (2006). Dust nuclei are considered to have ice nucleating properties as deduced from laboratory studies for montmorillonite. Montmorillonite initiates contact and immersion freezing at rather high temperatures so that freezing by black carbon is less important

and the glaciation indirect effect is negligible (Lohmann and Diehl, 2006). Black carbon and dust in internally mixed particles are involved in immersion freezing, whereas the externally mixed black carbon and dust aerosols participate in contact freezing.

At subfreezing temperatures the vapor pressure over ice is lower than over water. This causes ice crystals in mixed-phase clouds to grow at the expense of cloud droplets (Bergeron-Findeisen process). The Bergeron-Findeisen process is parameterized such that a supercooled water cloud will glaciate once a threshold ice water content of 0.5 mg $kg^{-1}$ is exceeded. Before sufficient ice has been formed due to heterogeneous freezing, saturation with respect to water is assumed in accordance with observations by Korolev and Isaac (2006). Once this threshold is exceeded, the remaining cloud water will be forced to evaporate and be deposited onto the existing ice crystals within that timestep and saturation with respect to ice is assumed. This differs from ECHAM4 and from the operational version of ECHAM5 (ECHAM5-REF) where depositional growth of ice crystals only takes place in the next time step if the air is still supersaturated with respect to ice. The remaining cloud droplets have to freeze or grow to rain drops but their evaporation within the time step and subsequent depositional growth of the ice crystals is not intended.

ECHAM4 includes a parameterization scheme for homogeneous and heterogeneous freezing in cirrus clouds (Lohmann and Kärcher, 2002) and allows supersaturation with respect to ice. As explained in Sect. 5, this cirrus scheme has not yet been implemented in ECHAM5. In the meantime, the saturation adjustment scheme is applied for all clouds in ECHAM5. The ice crystal number concentration at temperatures below –35°C is obtained from the newly deposited ice water by prescribing the effective ice crystal size following Lohmann (2002b) and applying Eqs. (4) and (5) described below. For depositional growth in cirrus clouds the assumption of spherical crystals is justified (Lohmann and Kärcher, 2002). The effective ice crystal size for newly formed crystals is assumed to depend on temperature. While it was based on observations from mid-latitude cirrus by Ou and Liou (1995) in ECHAM4, here we use the newer parameterization by Boudala et al. (2002), because the parameterization by Ou and

Liou (1995) yields negative ice crystal sizes at temperatures below –73°C.

### 2.3 Cloud optical properties

Cloud optical properties are formulated in terms of the cloud liquid and ice mass mixing ratios and their effective radii. Both in ECHAM4 and in the ECHAM5 simulations with the double-moment cloud microphysics scheme, the effective radius for cloud droplets is obtained from the mean volume radius and a simple parameterization of the dispersion effect that depends on the cloud droplet number concentration (Peng and Lohmann, 2003).

The effective ice crystal radius $r_i$ is not easy to obtain from in-situ observations because measurements of small ice crystals are not yet reliable (Field et al., 2003). Thus, parameterizations that relate ice crystal size to ice water content or temperature yield vastly different results. In ECHAM5, $r_i$ is empirically related to the ice water content (Lohmann and Roeckner, 1995):

$$r_i = 83.8 \cdot IWC^{0.216} \tag{3}$$

where $IWC$ is given in g m$^{-3}$ and $r_i$ in $\mu$m.

In ECHAM4 an empirical relationship between the mean volume radius $r_v$ and the effective radius (S. Moss, personal communication, and Lohmann, 2002b) has been used:

$$r_i = 1.61 r_v^3 + 3.56 \cdot 10^{-4} r_v^6 \tag{4}$$

where $r_v$ is obtained from the cloud ice mixing ratio in the cloudy part of the grid box $q_i$ and the ice crystal number concentration $N_i$:

$$r_v = \left( \frac{3 q_i \rho_a}{4 \pi \rho_i N_i} \right)^{1/3} \tag{5}$$

where $\rho_a$ = air density and $\rho_i$ = ice density (500 kg m$^{-3}$).

Equation (5) is problematic because it assumes that the ice crystals are spherical. This assumption may be justified for newly formed ice crystals in cirrus clouds at cold temperatures but is not supported by observations in mid-latitude ice clouds that are warmer than –40°C (Korolev and Isaac, 2003). Equations (4) and (5) yield considerably smaller ice crystals than using Eq. (3), which has a profound effect on the radiation balance. It results in a much larger longwave cloud forcing and too little outgoing longwave radiation. In order to re-adjust the radiation balance, the aggregation rate of ice crystals to form snow flakes needs to be artificially enhanced. This unrealistically reduced the ice water content as discussed below.

### 2.4 Set-up of the simulations

We compare different simulations with ECHAM5 as summarized in Table 1. These simulations are conducted in order to understand the importance of the double-moment cloud microphysics scheme including the revised parameterization of the Bergeron-Findeisen process on the present-day climate and to evaluate the impact of the cloud cover scheme and the aerosol emission inventory for the anthropogenic aerosol effect.

The ECHAM5 simulations have been carried out in T42 horizontal resolution (2.8125°×2.8125°) and 19 vertical levels. All simulations had the model top at 10 hPa and used climatological sea surface temperature and sea-ice extent. They were simulated for 5 years after an initial spin-up of 3 months using aerosol emissions for the year 2000. To isolate the anthropogenic effect, the simulations with the double-moment cloud microphysics scheme were repeated with aerosol emissions representative for the year 1750 (Dentener et al., 2006). There is no pre-industrial simulation for ECHAM5-REF because the aerosols in ECHAM5-REF do not affect cloud properties and, hence, cause no aerosol indirect effect.

These simulations are compared to a simulation with ECHAM4 that uses the same double-moment cloud microphysics scheme except for the changes discussed above. Both ECHAM4 and ECHAM5-HAM assume that dust aerosols initiate freezing at the temperatures that have been obtained from montmorillonite dust particles in the labora-

tory (Lohmann and Diehl, 2006). The simulations with ECHAM4 were carried out over 10 years in T30 horizontal resolution with 19 vertical levels with present-day aerosol emissions representative for the year 1985.

## 3 Model evaluation

An overview of the global-mean radiation and water budget is given in Table 2. The ECHAM5 simulations with the double-moment cloud microphysics scheme are conducted such that the global annual mean radiation budget is balanced to within 1 W m$^{-2}$ at the top-of-the-atmosphere (TOA) and that the values of the shortwave and longwave cloud forcing are within the uncertainty of the radiative flux measurements of ±5 W m$^{-2}$ as reported by Kiehl and Trenberth (1997).

Liquid water path cannot be retrieved reliably so that the satellite estimates vary substantially. They range between 50-84 g m$^{-2}$ in the global annual mean over the oceans as deduced from various SSM/I data (Ferraro et al., 1996; Greenwald et al., 1993). All model simulations have values within this range. It is even more difficult to derive an ice water path from satellites. Therefore the total water path (sum of liquid and ice water path) over both land and oceans is shown. It is estimated between 64 g m$^{-2}$ from ISCCP (Rossow and Schiffer, 1999) and 150–155 g m$^{-2}$ from the MODIS sensors on board the Aqua and the Terra satellites (King et al., 2003). Again all model simulations fall within this wide range.

The vertically integrated cloud droplet number concentration was derived by Han et al. (1998) from ISCCP data between 50° S and 50° N for 4 months (January, April, July, October) in 1987, the average of which can be considered as an annual mean. It amounts to $4\times10^{10}$ m$^{-2}$ and is simulated best in ECHAM5-RH. Employing 1985 emissions worsens the agreement as discussed in more detail below. However, even the ECHAM5-1985 simulation agrees much better with the observations than ECHAM4. It is a result of the different vertical aerosol number concentration as explained below. The cloud top effective cloud droplet radii of warm clouds with cloud top temperatures

above 0°C agree within 1.5 $\mu$m with the observed ones derived from ISCCP data between 50° S and 50° N by Han et al. (1994).

The vertically integrated ice crystal number concentration is rather similar in the ECHAM5 simulations. Due of the different approach to obtain the effective ice crystal radius in ECHAM4 that necessitates a smaller ice water path (see Sect. 2), its ice crystal number concentration is less than 10% of the concentrations in ECHAM5. Unfortunately there are no global observations of the ice crystal number concentrations. Thus, we cannot conclude which global estimate is best. We will, however, compare the ice water content and number concentrations in mid latitudes with observations in Sect. 3.2.

The total cloud cover in ECHAM5-RH is smaller than in ECHAM4 due to the absence of the cirrus scheme (Table 2). It is at the high side of the satellite retrievals (Rossow and Schiffer, 1999) and surface observations (Hahn et al., 1994) in ECHAM4, but in the mid-range of the observations in the ECHAM5 simulations. While precipitation was underestimated in ECHAM4 it is overestimated in all ECHAM5 simulations due to more vigorous convection in ECHAM5 as discussed below.

The cloud radiative forcing is defined as the difference in the total sky shortwave or longwave minus the clear sky shortwave or longwave radiation. The shortwave cloud forcing (SCF) has been estimated from ERBE satellites to amount to –50 W m$^{-2}$ and the longwave cloud forcing (LCF) to 30 W m$^{-2}$ (Kiehl and Trenberth, 1997). However, LCF estimates from the TOVS satellites only amount to 22 W m$^{-2}$ (Susskind et al., 1997; Scott et al., 1999), which provides an estimate of the measurement uncertainties. In ECHAM4 SCF amounted to only –46.4 W m$^{-2}$, while it is 1–3 W m$^{-2}$ larger than observed in ECHAM5-RH and ECHAM5-1985 as a result adjusting the model to match the global mean radiation balance at the top-of-the-atmosphere. On the contrary, the longwave cloud forcing is smaller in the ECHAM5 simulations than in ECHAM4. All ECHAM5 values fall between the ERBE and TOVS estimate of LCF (Table 2).

The aerosol optical depth from all ECHAM5 simulations falls within the observed uncertainty (see also Stier et al., 2005), whereas AOD is severely underpredicted in

ECHAM4. There is a slight increase in AOD from 0.165 in ECHAM5-COV to 0.173 in ECHAM5-RH resulting from slightly less precipitation in ECHAM5-RH that removes fewer aerosols from the atmosphere.

### 3.1 Annual, zonal means

Annual zonal means of the oceanic liquid water path, total water path, total cloud cover, precipitation, shortwave and longwave cloud forcing, aerosol optical depth, water vapor mass and vertically integrated number concentration of cloud droplet and ice crystals are shown in Fig. 1. The aerosol optical depth (AOD) is much smaller in ECHAM4 than in ECHAM5 and has a different latitudinal distribution than in both ECHAM5 and in the observations. The contribution of sea salt and biomass burning are much larger in ECHAM5 than in ECHAM4, whereas ECHAM4 predicts more Arctic haze. The reduced poleward transport in ECHAM5 results from the less diffuse new advection scheme for water vapor, cloud variables and aerosols employed in ECHAM5 (Roeckner et al., 2003). As compared to the MODIS retrievals of aerosol optical depth, although the meridional distribution is well captured in ECHAM5, it overpredicts AOD over the Southern Ocean. On the contrary, AOD in ECHAM4 is much lower than observed everywhere but has hints of Arctic haze as suggested in the observations. There is, however, still some discrepancy between different aerosol optical depth estimates (Kinne, 2007[1]) with the merged MODIS-MISR satellite estimate shown here being the best estimate.

The liquid water path distribution is also markedly different between ECHAM4 and ECHAM5. Whereas the liquid water path has its maximum in the tropics in ECHAM4, liquid water path is largest in the mid latitudes in all ECHAM5 simulations. The liquid water path in the different ECHAM5 simulations varies in magnitude, but its latitudinal pattern is similar. Outside the tropics it falls within the observational uncertainty range. In the mid-latitudes the liquid water path is higher in the ECHAM5 simulations with

[1]Kinne, S.: Aerosol Direct Radiative Forcing with an AERONET touch, Atmos. Environ., submitted, 2007.

the double-moment cloud microphysics scheme than in ECHAM5-REF due to aerosol-cloud coupling. The ECHAM5 simulations with the double moment cloud microphysics scheme apply the autoconversion rate from Khairoutdinov and Kogan (2000), which inversely depends on the cloud droplet number concentration. Thus, as the aerosol number concentration determines the cloud droplet number concentration, an increase in aerosol and, hence, cloud droplet number concentration prolongs the precipitation formation rate, leading to a higher liquid water path and a reduced removal of aerosols (see also Lohmann and Feichter, 1997).

The decrease in liquid water path in the tropics results from larger tropical precipitation efficiency in ECHAM5 than in ECHAM4. Even though the convection scheme has not changed from ECHAM4 to ECHAM5, the frequency of deep convection has increased from ECHAM4 to ECHAM5 because the longwave cooling rates are larger in the tropical upper troposphere with the introduction of the new longwave radiation scheme in ECHAM5. Moreover, the increase from two wavelength bands in the shortwave radiation in ECHAM4 to six wavelength bands in ECHAM5 reduces the absorption of shortwave radiation in the atmosphere considerably (Wild and Roeckner, 2006). This enhanced cooling and reduced shortwave heating destabilizes the atmosphere causing more frequent deep convection events in ECHAM5. Thus, the global mean precipitation and especially the convective precipitation rate is systematically higher and the water vapor mass lower in ECHAM5 as compared to ECHAM4 (Table 2 and Fig. 1). In turn, tropical shallow convection occurs less often in ECHAM5 so that less cloud water is detrained from these clouds. Hence, the maximum in liquid water path in the tropics is reduced from ECHAM4 to ECHAM5. The secondary liquid water path maximum in the tropics is best simulated in ECHAM5-1985 as a result of the higher aerosol emissions and AOD in the tropics. Because of the higher aerosol levels, these tropical clouds contain more but smaller cloud droplets that precipitate less efficiently.

In terms of the total water path, all simulations fall in between the estimates from the ISCCP and MODIS satellites except polewards of 60°, where the satellite estimates are less reliable. The lowest values outside the tropics stem from the ECHAM4 simulation

because of its very low ice water path and from ECHAM5-REF because of its lowest liquid water path.

The vertically integrated cloud droplet number concentration agrees well with observations in all ECHAM5 simulations with the double moment cloud microphysics scheme, but exceeds the observed concentration globally by a factor of 5 in ECHAM4 (cf. Table 2). Because the cloud droplet and ice crystal number concentrations are not predicted in ECHAM5-REF, they are absent from the figures and the table. When the 1985 aerosol emissions are used, more cloud droplets than observed are simulated in the tropics and Northern Hemisphere midlatitudes. The higher cloud droplet number concentration in these regions reflects the higher carbonaceous aerosol emissions over Europe, south-east Asia and South and North America in the 1985 emission inventory.

Differences in the vertically integrated ice crystal number concentration are most apparent in the tropics and over the South Pole. While the ice crystal number concentration does not exceed $0.3\times10^{10}\,m^{-2}$ anywhere in ECHAM4, it increases to more than $3\times10^{10}\,m^{-2}$ in ECHAM5-COV in the tropics and over Antarctica. All other simulations fall in between. As mentioned above no global estimates are available of the ice crystal number concentration and even locally large uncertainties remain because of the difficulty with measuring small ice crystals (Field et al., 2003).

Because of the more vigorous precipitation and lower total water path in the tropics in the ECHAM5 simulations, the cloud cover, and the shortwave and longwave cloud forcing are also smaller in the tropics in the ECHAM5 simulations as compared to ECHAM4. Over mid-latitudes, where the liquid water path is generally larger in the ECHAM5 simulations as compared to ECHAM4 due to the higher aerosol and, hence, cloud droplet number concentration, the shortwave cloud forcing is larger in the ECHAM5 simulations, in better agreement with the observations. The reduction in longwave cloud forcing in the ECHAM5 simulations in the tropics falls in between the longwave cloud forcing estimates from ERBE and from TOVS.

### 3.2 Annual latitude-pressure cross sections

In order to better understand the large differences between ECHAM4 and ECHAM5-RH, annual zonal mean plots of the aerosol number $N$ concentration available for droplet nucleation ($N$ with $r>0.035\,\mu$m), liquid and ice water contents (LWC, IWC) of stratiform clouds, cloud droplet and ice crystal number concentrations, and cloud cover are shown as a function of altitude in Fig. 2. Most noticeable is the vastly different vertical distribution of the aerosol number concentration. In ECHAM4, the aerosol number concentration is higher in the boundary layer, because it assumes externally mixed aerosols of different sizes, which are, on average, smaller than the accumulation size aerosols in ECHAM5. On the contrary, the aerosol number concentration is larger at higher altitudes in ECHAM5-HAM than in ECHAM4. In ECHAM5-HAM secondary particles are formed in the upper free troposphere by nucleation, a pathway that is missing in ECHAM4. The upper free tropospheric new particle formation is a major contributor to the particle number, some of which subsequently grow to sizes larger than 0.035 $\mu$m as seen in Fig. 2. In addition the 2000 emission inventory includes wildfires and biomass burning which are injected up to a height of 6 km (Dentener et al., 2006) whereas in the 1985 emission inventory used in ECHAM4, biomass burning emissions where only distributed over the first and second model level above the surface. Lastly, the scavenging of aerosols from convective clouds has changed between ECHAM4 and ECHAM5-HAM in which now mode specific semi-empirical scavenging coefficients are employed (Stier et al., 2005).

Despite higher aerosol concentrations in the mid and upper troposphere, the cloud droplet number concentration is almost everywhere lower in ECHAM5-RH. In the boundary layer this is consistent with the smaller aerosol number concentration. In the mid troposphere the cloud droplet number concentration has decreased in favor of the ice crystal number concentration as the Bergeron-Findeisen process is more efficient in ECHAM5-RH. This is in better agreement with in-situ data as discussed in the next subsection. The increase in cloud ice in ECHAM5-RH results partly from the more effi-

cient Bergeron-Findeisen process but is also a result of the larger ice crystal sizes. As explained in Sect. 2, the larger ice crystals are less reflective for a given ice water path. Thus, in order to match the longwave cloud forcing, the ice water path can be higher in ECHAM5 with larger crystals than in ECHAM4 where the ice crystals are smaller. The cloud cover is smaller in ECHAM5-RH as compared to ECHAM4 especially in the upper troposphere due to the absence of the cirrus scheme in ECHAM5-RH.

### 3.3 Comparison with field data

There is a caveat when trying to validate climate model output with data from field experiments because a climate model cannot be expected to capture individual events. Nevertheless, they are the best observations available for the validation of aerosol and cloud properties within the atmosphere.

#### 3.3.1 Aerosols

Figure 3 shows observed vertical profiles plus error bars of the black carbon mass and the total aerosol mass from Houston, Texas (Schwarz et al., 2006) in November 2004. The thermal tropopause was observed to be near 150 hPa. We selected the same data plus their 25% and 75% percentiles from each November of the simulation in the region between 29–38° N and 88–98° W that encompasses the aircraft flights. There is almost no difference in the total aerosol mass in all ECHAM5 simulations. The observed vertical distribution is well reproduced in ECHAM5 and all simulations fall within the measurement uncertainty at altitudes below 100 hPa. Above that level, the aerosol concentrations in all ECHAM5 simulations are on the low side. This is probably due to convective scavenging because it controls the upper troposphere/lower stratosphere (UTLS) aerosol concentrations.

ECHAM4 has a completely different vertical profile than all the ECHAM5 simulations. While the ECHAM4 25% and 75% percentiles encompass the observations below 300 hPa, the aerosol mass rapidly decreases with altitude and drastically under-

estimates the observations above 300 hPa. The improved representation of the UTLS aerosol concentration in ECHAM5 is indicative of the importance of aerosol nucleation and the subsequent microphysical growth included in the aerosol module HAM. The larger aerosol concentrations in ECHAM4 than in ECHAM5 below 500 hPa stem from differences in emissions and different removal rates.

In terms of the black carbon mass mixing ratio, there is hardly any difference between the simulations ECHAM5-REF, ECHAM5-RH and ECHAM5-COV and they fall within the measurement uncertainty in the troposphere. The ECHAM5-1985 simulation has a higher black carbon mass mixing ratio because of its higher black carbon emissions. Again, ECHAM4 has a completely different vertical profile than all the ECHAM5 simulations with a higher black carbon mass below 200 hPa and less black carbon aloft.

In the stratosphere, all ECHAM5 simulations overestimate the black carbon mass whereas the total aerosol mass was underestimated. This suggests that other aerosol species but black carbon are more efficiently removed from the atmosphere. The same relative behaviour can be noticed in ECHAM4, where the underprediction in black carbon mass in the stratosphere is less severe than for the total aerosol mass.

### 3.3.2 Cloud properties

In terms of the validation of cloud properties, we compare LWC, IWC and total water content (TWC) of stratiform clouds as a function of temperature between 0°C and –35°C with stratiform cloud observations taken from different field projects over Canada in winter, spring and fall (Korolev et al., 2003). We took model data from one year in the same months (December–April, September/October) and the same region as the observations were taken.

In the observations, the distinction between ice and liquid is based on the ratio of IWC to TWC from separate measurements of the liquid and total water content with different sensors of the Nevzorov probe (Korolev et al., 1998). Clouds are considered liquid when the ratio IWC/TWC is less than 10% and ice, when the ratio IWC/TWC exceeds 90% (Korolev et al., 2003).

The increases in LWC, IWC and TWC for clouds with TWC >0.003 g m$^{-3}$ as a function of temperature is shown in Fig. 4. Whereas the observed LWC increases from 0.017 g m$^{-3}$ at –33°C to 0.1 g m$^{-3}$ at –2°C, the increase in IWC with temperature is more modest. The observed IWC has a weak maximum of 0.04 g m$^{-3}$ at ∼–12°C where depositional growth is most effective. At –20°C a cross-over from more LWC at higher temperatures to more IWC at lower temperatures is observed.

While one needs to compare grid-average values of cloud water path with satellite data, for the comparison with in-situ measurements the in-cloud values of LWC, IWC and TWC, i.e. the water contents within the cloudy part of the grid box are used. The increases in LWC, IWC and TWC are rather similar in the ECHAM5 simulations with the double moment cloud microphysics scheme. They mimic the observed modest change in IWC with temperature and the steady increase in LWC and TWC with temperature, but the temperature at which LWC and IWC cross over is lower than observed. ECHAM5-REF overestimates LWC at the expense of IWC because of its less efficient Bergeron-Findeisen process (see Sect. 2).

The much lower IWC in ECHAM4 results from the smaller ice crystals (Eqs. 4 and 5). Because the ice cloud is more reflective and traps more longwave radiation when the crystals are smaller for a given ice water content, the aggregation rate of ice crystals to form precipitation size particles had to be enhanced. This depletes the ice water content as shown in Fig. 4. This suggests that it is better to use Eq. (3) which is the basis for all ECHAM5 simulations. As discussed above Eq. (5) is problematic to use because it assumes that the ice crystals are spherical, which is not justified in mid-latitude ice clouds that are warmer than –40°C (Korolev and Isaac, 2003). LWC in ECHAM4 is highly overestimated between –15 and –20°C with 0.8 g m$^{-3}$ because of the inefficient Bergeron-Findeisen process.

The probability distributions of mixed-phase cloud composition for clouds with TWC >0.003 g m$^{-3}$ for different temperature intervals is shown in Fig. 5. It is apparent from the observations that clouds tend to be composed to more than 90% of water or to more than 90% of ice due to the Bergeron-Findeisen process. The higher occurrence

of IWC/TWC between 0.6 to 0.9 seems to be rather a measurement problem (A. Korolev, personal communication, 2006). As expected, the occurrence of a high percentage of ice is more likely at colder temperatures whereas at warmer temperatures clouds mainly composed of water. While all ECHAM5 simulations with the double-moment cloud microphysics scheme overpredict the occurrence of almost pure ice clouds at colder temperatures, ECHAM4 underestimates high IWC, and both ECHAM4 and ECHAM5-REF overestimate the occurrence of almost pure water clouds due to their smaller ice water content.

The cloud droplet and ice crystal number concentrations with diameters between 5–95 $\mu$m are shown as a function of temperature in Fig. 6. The observations stem from the forward scattering spectrometer probe (FSSP) that traditionally measures cloud droplets, but has also been used to measure ice crystal number concentrations, even though it has some caveats (Korolev et al., 2003). The observations show the highest particle concentrations for a IWC/TWC ratio <0.1, which is indicative of almost pure water clouds. As the IWC/TWC ratio increases, fewer particles are observed especially in case of IWC/TWC >0.9, which is indicative of almost pure ice clouds.

The comparison of the ECHAM5 simulations with observations yields that the cloud droplet number concentration is generally well simulated and a significant improvement over ECHAM4. However, all ECHAM5 simulations except ECHAM5-COV overestimate the particle concentration at the highest IWC/TWC pointing to an overestimate of the ice crystal number concentration. Also, the particle concentrations for intermediate IWC/TWC ratios >0.5 are higher than observed in all simulations. This suggests that we have more droplets with higher number concentrations and fewer ice crystals with smaller number concentrations in these clouds.

The particle number concentrations from the ECHAM5 simulations agree better with observations than from ECHAM4. In ECHAM4, the cloud droplet number concentration is underestimated in mixed-phase clouds despite having a much larger vertically integrated cloud droplet number concentration (cf. Table 2) because the liquid water clouds with the highest cloud droplet number concentration occur at lower altitudes

in ECHAM4 as compared to ECHAM5-RH (cf. Fig. 2). The particle concentrations for higher IWC/TWC ratios are even closer together at temperatures above –10°C in ECHAM4 as compared to ECHAM5. At colder temperatures there is some spread in ECHAM4 but the ice crystal concentrations (IWC/TWC >0.9) are severely underestimated at temperatures below –20°C.

## 4 The anthropogenic aerosol effect in ECHAM5-HAM

The annual global mean changes in the radiative budget at TOA and of the hydrological cycle from pre-industrial times to present-day are summarized in Table 3. The total anthropogenic aerosol effect defined as the difference in the net TOA radiation includes contributions from the direct aerosol effect, the cloud albedo effect, the cloud lifetime effect, the semi-direct effect and the glaciation effect. However, the contribution from the glaciation effect when treating dust as montmorillonite is rather small (Lohmann and Diehl, 2006) as is the contribution from the direct effect, which amounts to –0.27 W m$^{-2}$ in ECHAM5-HAM (Schulz et al., 2006).

As summarized in Table 3, the increase in cloud cover is largest in simulation ECHAM5-COV that uses the statistical cloud cover scheme (Tompkins, 2002) and in ECHAM5-1985. In ECHAM5-COV, this stems from the tighter coupling of the cloud water content and cloud cover in the Tompkins scheme. Here an increase in cloud cover reduces the in-cloud liquid water content, which in turn reduces the autoconversion rate and, hence, increases cloud cover in the next timestep. Along the same lines, Lohmann and Feichter (1997) obtained a much larger indirect effect when the relative humidity-based cloud cover scheme by Sundqvist et al. (1989) was replaced by the semi-empirical cloud cover scheme by Xu and Randall (1996) that uses both relative humidity and cloud water content as predictors for cloud cover. In ECHAM5-1985, the increase in the cloud droplet number concentration and the liquid water path is the largest of the ECHAM5 simulations and the global mean precipitation decreases the most. This results in a higher relative humidity, which in turn also increases the cloud

cover.

The smaller increase in cloud cover and liquid water path in ECHAM5-RH entails a smaller decrease in the TOA shortwave radiation of –2 W m$^{-2}$ that is comparable to the –1.8 W m$^{-2}$ in ECHAM4. Because of the larger cloud cover and liquid water path increase in ECHAM5-COV and ECHAM5-1985, their decreases in shortwave radiations amount to –3.2 W m$^{-2}$ and –3.1 W m$^{-2}$, respectively.

In ECHAM4, the increase in the number of supercooled aerosols available for cirrus formation causes an increase in the cirrus ice crystal number concentration, hence reducing the outgoing longwave radiation by 0.7 W m$^{-2}$ (Table 3). Because the cirrus scheme is not yet implemented in ECHAM5, the decrease in longwave radiation only amounts to 0.2 to 0.4 W m$^{-2}$, thus compensating less of the reduction in shortwave radiation.

Thus, the anthropogenic aerosol effect, defined as the difference in the net TOA radiation amounts to between –1.8 and –2.9 W m$^{-2}$ in the ECHAM5 simulations. This is more than 80% larger than the –1 W m$^{-2}$ obtained with ECHAM4.

The annual zonal mean latitude versus pressure differences of the aerosol number concentration >0.035 $\mu$m, the grid-box averaged cloud droplet and ice crystal concentration, LWC, IWC, and cloud cover from ECHAM4 and from ECHAM5-RH are shown in Fig. 7. Whereas the increase in the anthropogenic aerosol number concentration is rather uniform in the vertical in the Northern Hemisphere mid-latitudes in ECHAM5-RH, the increase in the anthropogenic aerosol number concentration is larger in ECHAM4 and is more confined to lower levels. The higher anthropogenic aerosol number concentration in the upper troposphere in ECHAM5-RH stems from homogeneous nucleation of sulfuric acid in ECHAM5-RH, a process that has not been considered in ECHAM4. On the contrary the 1985 emissions of black and organic carbon exceed the 2000 emissions by 50% and more than 100%, respectively, and cause the higher aerosol number concentrations below 600 hPa in ECHAM4.

As a consequence of the difference in the aerosol number concentration, the increases in CDNC and LWC in ECHAM4 are larger in the lower and mid troposphere

as compared to ECHAM5-RH. The ice crystal number concentration and IWC increase between 400 and 200 hPa in ECHAM4, especially on the Northern Hemisphere because it includes homogeneous freezing of supercooled aerosols for the formation of cirrus clouds. Because of the absence of the homogeneous freezing scheme in ECHAM5-RH, the increases and decreases in ice crystal number concentration and ice water content reflect the more arbitrary changes in cloud cover.

The latitudinal distributions of the changes in AOD, the hydrological cycle and in the radiation balance between pre-industrial times and present-day are shown in Fig. 8. The increase in aerosol optical depth occurs further poleward in ECHAM4 because ECHAM4 predicts more Arctic haze in the present-day climate.

The increase in liquid water path does not mimic the increase in AOD because the increase in liquid water path stems from the retardation of the drizzle formation which depends on the cloud susceptibility. Clouds are most susceptible to changes in aerosol concentration where background cloud droplet number concentrations are the smallest, i.e. over the remote oceans. Thus, the increase in liquid water path extends further poleward than the increase in AOD. Moreover, the peaks in the increase in tropical liquid water path in simulations ECHAM5-1985 and ECHAM4 are more pronounced than the change in AOD. They result from the higher biomass burning emissions in the 1985 emission inventory. More aerosols in the tropics cause higher cloud droplet number concentrations in the detrained cloud water from convective clouds so that the stratiform part of these clouds precipitates less (Fig. 8).

The changes in ice water path and total cloud cover are rather noisy and do not change systematically in ECHAM5-RH and ECHAM4. A consistent increase in liquid water path, ice water path and total cloud cover is apparent in simulation ECHAM5-COV in Northern Hemisphere mid latitudes for the reasons explained above.

The increase in the cloud droplet number concentration is larger in ECHAM5-1985 than in ECHAM5-RH despite its anthropogenic AOD increase being the lowest (Table 3 and Fig. 8). This is caused by the different vertical structure of the aerosol emissions in the 1985 and 2000 emission inventories (see Sect. 3.2). In ECHAM5-1985, as in

ECHAM4, the increase in aerosol number concentration is more limited to the boundary layer, where most water clouds are. This leads to the large increase in the cloud droplet number concentration and liquid water path in ECHAM5-1985 that is comparable to ECHAM4. Yet, the total anthropogenic aerosol effect is larger in ECHAM5-1985 than in ECHAM4 because of the large increase in cloud cover over NH midlatitudes (Fig. 8).

The global mean precipitation is reduced most in ECHAM4 because the Bergeron-Findeisen process is smallest in this simulation as discussed in Sect. 3.3. The largest decrease in precipitation in ECHAM4 and ECHAM5-1985 occurs at the equator. Because more cloud water is then detrained, it causes the large increase in liquid water path in the tropics in these simulations. On the contrary, the more moderate increase in liquid water path in ECHAM5-RH and ECHAM5-COV in the tropics is a result of an increase in convective precipitation (not shown).

The indirect aerosol effect can be separated into the purely radiative cloud albedo effect, which is a change in the net shortwave radiation resulting from a decrease in the cloud top effective radius and the cloud lifetime effect. As shown in Fig. 8, the cloud top effective radius sampled only over cloudy periods within the cloudy part of the grid box decreases between 0.3 and 0.6 $\mu$m in mid latitudes of the Northern Hemisphere. The maximum decrease in the effective radius in ECHAM5-RH and ECHAM5-COV occurs between 35 and 50° N where the anthropogenic aerosol emissions are largest.

However, this decrease in cloud top radius is only part of the explanation for the decrease in the TOA shortwave radiation because smaller cloud droplets retard the precipitation formation and cause the built-up of cloud water as seen in Fig. 8. The combined changes in cloud top effective radius, liquid water path and total cloud cover then explain the changes in TOA shortwave radiation. Its decrease is smallest in ECHAM4 because cloud cover changed the least in this simulation. On the other hand, in ECHAM5-COV and ECHAM5-1985, where the increases in cloud cover are largest, the decreases in shortwave radiation are the largest, exceeding 5 W m$^{-2}$ in the mid-latitudes of the Northern Hemisphere.

Decreases in outgoing longwave radiation are most pronounced at Northern Hemi-

sphere mid and high latitudes in ECHAM4 following the slight increase in ice water path here. As discussed above, the changes in outgoing longwave radiation are smaller in ECHAM5 due to the absence of the cirrus scheme. Consequently the changes in net radiation are rather similar to the changes in shortwave radiation in the ECHAM5 simulations. In ECHAM4, on the other hand, the change in TOA net radiation is generally smaller. The TOA net radiation in ECHAM4 is actually increased in the Arctic in the present-day climate because of longwave effects.

## 5 Conclusions

The double-moment cloud microphysics scheme of ECHAM4 has been coupled to the size-resolved aerosol scheme ECHAM5-HAM. The major differences between the model set-ups in ECHAM4 and the ECHAM5 version used in this study can be summarized as follows:

- ECHAM5-HAM predicts the aerosol mass and number concentration and the aerosol mixing state (Stier et al., 2006), whereas an externally mixed aerosol number concentration was obtained from the prediction of their different mass mixing ratios in ECHAM4 (Lohmann, 2002b). ECHAM5-HAM also considers homogeneous nucleation of sulfuric acid in the upper troposphere and the subsequent microphysical growth, which is missing in ECHAM4.
- ECHAM5 has the option of employing a new cloud cover scheme that takes the subgrid-scale variability into account (Tompkins, 2002). However, the cirrus scheme (Lohmann and Kärcher, 2002) has not yet been introduced as explained below.
- The ECHAM5 radiation scheme has changed. It has more spectral bands in both the longwave and the shortwave wavelengths (Roeckner et al., 2003). It also employs a new longwave radiation code that is based on the two-stream approximation instead of the emissivity method applied in ECHAM4.

– The transport scheme for positive definite variables (water vapor, gases, aerosols, and cloud variables) has been improved. It is mass-conserving and shape-preserving in ECHAM5 (Lin and Rood, 1996).

The introduction of the new aerosol microphysics scheme results in a vast increase in aerosol optical depth from ECHAM4 to ECHAM5. The aerosol optical depth in all ECHAM5 simulations is in much better agreement with observations. The ECHAM5 aerosol microphysics scheme including homogeneous nucleation of sulfuric acid in the upper troposphere yields a much better vertical aerosol distribution over continental North America.

The introduction of the new radiation scheme leads to more longwave cooling in the tropical upper troposphere. Combined with less absorption of shortwave radiation within the atmosphere, the atmosphere is less stable. The greater static instability requires more penetrative convection for compensation. This increases the global mean convective precipitation.

The liquid and ice water content as a function of temperature in mixed-phase clouds agree better with in-situ data from aircraft campaigns in midlatitudes in the ECHAM5 simulations with the double-moment cloud microphysics scheme than in ECHAM4. This is partly caused by the different empirical formulas for the effective ice crystal radius and partly due to the more efficient Bergeron-Findeisen process in the ECHAM5 simulations with the double-moment cloud microphysics scheme. The cloud droplet and ice crystal number concentrations are also better simulated partly because the aerosol number concentration available for droplet nucleation is more realistic and partly because of the more efficient Bergeron-Findeisen process.

The total anthropogenic aerosol effect defined as the difference in the top-of-the-atmosphere net radiation between present-day and pre-industrial times amounts to $-1.8\,\mathrm{W\,m^{-2}}$ in simulation ECHAM5-RH (cf. Table 3), when the relative humidity based cloud cover scheme (Sundqvist et al., 1989) and present-day aerosol emissions representative for the year 2000 are used. It is larger when either a statistical cloud cover scheme (Tompkins, 2002) or when a different aerosol emissions inventory, that has

higher biomass burning emissions, are used. The total anthropogenic aerosol effect is larger when using the Tompkins (2002) scheme because an increase in cloud condensate entails an increase in cloud cover. The aerosol effect is larger when the 1985 aerosol emissions are used because in that emission inventory the black and organic carbon emissions are 50% and 120% larger than in the 2000 aerosol emission inventory. The net anthropogenic aerosol effect at the top-of-the-atmosphere is larger in ECHAM5-RH than in ECHAM4 while the decrease in shortwave radiation is comparable in both simulations. The larger decrease in the net radiation in ECHAM5-RH is due to the absence of the cirrus scheme that causes a larger decrease in the longwave radiation in ECHAM4.

When the cirrus scheme was implemented in ECHAM4, the assumption was made that the cloud cover equals one when the relative humidity exceeds 100% and a cloud is present. While this is consistent with the assumption for warm and mixed-phase clouds, it is inconsistent for cirrus clouds where high supersaturations with respect to ice are a prerequisite for cirrus cloud formation. Similar to water clouds, the correct assumption would be that cirrus clouds can also form in part of the grid box only, even when the grid-mean relative humidity exceeds 100% (Tompkins et al., 2007). Because this approach is not straight forward in the context of the Tompkins (2002) cloud cover scheme, it was not implemented for the simulations described above, but will be done in the future.

*Acknowledgements.* The authors are grateful for financial support from NCCR Climate. They thank J. Quaas and S. Kinne for providing satellite data, A. Korolev for providing the in-situ aircraft data, S. Kloster for providing aerosol emissions and the German Computing Centre (DKRZ) for computing time.

## References

Ackerman, A. S., Toon, O. B., Stevens, D. E., Heymsfield, A. J., Ramanathan, V., and Welton, E. J.: Reduction of tropical cloudiness by soot, Science, 288, 1042–1047, 2000. 3721

Albrecht, B.: Aerosols, Cloud Microphysics, and Fractional Cloudiness, Science, 245, 1227–1230, 1989. 3721

Boucher, O. and Lohmann, U.: The sulfate-CCN-cloud albedo effect: A sensitivity study with two general circulation models, Tellus, Ser. B, 47, 281–300, 1995. 3720

Boudala, F. S., Isaac, G. A., Fu, Q., and Cober, S. G.: Parameterization of effective ice particle size for high-latitude clouds, Int. J. Climatol., 22, 1267–1284, 2002. 3726

Cagnazzo, C., Manzini, E., Giorgetta, M. A., and Forster, P.: Impact of an improved radiation scheme in the MAECHAM5 General Circulation Model, Atmos. Chem. Phys. Discuss., 6, 11 067–11 092, 2006. 3723

Dentener, F., Kinne, S., Bond, T., Boucher, O., Cofala, J., Generoso, S., Ginoux, P., Gong, S., Hoelzemann, J., Ito, A., Marelli, L., Penner, J., Putaud, J.-E., Textor, C., Schulz, M., van der Werf, G., and J., W.: Emissions of primary aerosol and precursor gases in the years 2000 and 1750 prescribed data-sets for AeroCom, Atmos. Chem. Phys., 6, 4321–4344, 2006, http://www.atmos-chem-phys.net/6/4321/2006/. 3724, 3728, 3734

Dusek, U., Frank, G. P., Hildebrandt, L., Curtius, J., Schneider, J., Walter, S., Chand, D., Drewnick, F., Hings, S., Jung, D., Borrmann, S., and Andreae, M. O.: Size matters more than chemistry for cloud-nucleating ability of aerosol particles, Science, 312, 1375–1378, 2006. 3724

Ferraro, R., Weng, F., Grody, N., and Basist, A.: An Eight Year (1987-1994) Time Series of Rainfall, Clouds, Water Vapor, Snow-cover, and Sea-ice Derived from SSM/I Measurements, Bull. Am. Meteorol. Soc., 77, 891–905, 1996. 3729, 3752

Field, P. R., Wood, R., Brown, P. R. A., Kaye, P. H., Hirst, E., Greenaway, R., and Smith, J. A.: Ice Particle Interarrival Times Measured with a Fast FSSP, J. Atmos Ocean. Techn., 20, 249–261, 2003. 3727, 3733

Greenwald, T. J., Stephens, G. L., Vonder Haar, T. H., and Jackson, D. L.: A Physical Retrieval of Cloud Liquid Water Over the Global Oceans Using Special Sensor Microwave/Imager (SSM/I) Observations, J. Geophys. Res., 98, 18 471–18 488, 1993. 3729, 3752

Hahn, C. J., Warren, S. G., and London, J.: Climatological data for clouds over the globe from sur- face observations, 1982–1991: The total cloud edition, Tech. rep., ORNL/CDIAC-72 NDP-026A Oak Ridge National Laboratory, Oak Ridge Tennessee, USA, 1994. 3730, 3752

Han, Q., Rossow, W. B., and Lacis, A. A.: Near-Global Survey of Effective Droplet Radii in Liquid Water Clouds Using ISCCP Data, J. Climate, 7, 465–497, 1994. 3730, 3752

Han, Q., Rossow, W. B., Chou, J., and Welch, R.: Global Variation of column droplet concen-

tration in low-level clouds, Geophys. Res. Lett., 25, 1419–1422, 1998. 3729, 3752
Jacobson, M. Z.: Effects of Externally-Through-Internally-Mixed Soot Inclusions within Clouds and Precipitation on Global Climate, J. Phys. Chem., 110, 6860–6873, 2006. 3722
Jones, A., Roberts, D. L., and Slingo, A.: A climate model study of indirect radiative forcing by anthropogenic sulphate aerosols, Nature, 370, 450–453, 1994. 3720
Khairoutdinov, M. and Kogan, Y.: A new cloud physics parameterization in a large-eddy simulation model of marine stratocumulus, Mon. Wea. Rev., 128, 229–243, 2000. 3732
Kiehl, J. T. and Trenberth, K. E.: Earth's Annual Global Mean Energy Budget, Bull. Am. Meteorol. Soc., 78, 197–208, 1997. 3729, 3730, 3752
King, M. D., Menzel, W. P., Kaufman, Y. J., Tanre, D., Gao, B. C., Platnick, S., Ackerman, S. A., Remer, L. A., Pincus, R., and Hubanks, P. A.: Cloud and aerosol properties, precipitable water, and profiles of temperature and water vapor from MODIS, IEEE Trans. Geo. Rem. Sens., 41, 442–458, 2003. 3729, 3752
Korolev, A. V. and Isaac, G. A.: Roundness and aspect ratio of particles in ice clouds, J. Atmos. Sci., 60, 1795–1808, 2003. 3728, 3737
Korolev, A. V. and Isaac, G. A.: Relative humidity in liquid, mixed-phase, and ice clouds, J. Atmos. Sci., 63, 2865–2880, 2006. 3726
Korolev, A. V., Strapp, J. W., Isaac, G. A., and Nevzorov, A. N.: The Nevzorov airborne hot-wire LWC-TWC probe: principle of operation and performance characteristics, J. Atmos. Ocea. Tech., 15, 1495–1510, 1998. 3736
Korolev, A. V., Isaac, G. A., Cober, S. G., Strapp, W., and Hallett, J.: Microphysical characterization of mixed-phase clouds, Q. J. R. Meteorol. Soc., 129, 39–65, 2003. 3736, 3738, 3757, 3758, 3759
Lin, H. and Leaitch, W. R.: Development of an in-cloud aerosol activation parameterization for climate modelling, in Proceedings of the WMO Workshop on Measurement of Cloud Properties for Forecasts of Weather, Air Quality and Climate, pp. 328–335, World Meteorol. Organ., Geneva, 1997. 3724
Lin, S. J. and Rood, R. B.: Multidimensional flux-form semi-Lagrangian transport schemes, Mon. Wea. Rev., 124, 2046–2070, 1996. 3723, 3744
Lohmann, U.: A glaciation indirect aerosol effect caused by soot aerosols, Geophys. Res. Lett., 29, 1052, doi:10.1029/2001GL014357, 2002a. 3721
Lohmann, U.: Possible aerosol effects on ice clouds via contact nucleation, J. Atmos. Sci., 59, 647–656, 2002b. 3723, 3725, 3726, 3727, 3743

Lohmann, U. and Diehl, K.: Sensitivity studies of the importance of dust ice nuclei for the indirect aerosol effect on stratiform mixed-phase clouds, J. Atmos. Sci, 63, 968–982, 2006. 3721, 3723, 3725, 3726, 3729, 3739, 3751

Lohmann, U. and Feichter, J.: Impact of sulfate aerosols on albedo and lifetime of clouds: A sensitivity study with the ECHAM GCM, J. Geophys. Res., 102, 13 685–13 700, 1997. 3732, 3739

Lohmann, U. and Feichter, J.: Global indirect aerosol effects: A review, Atmos. Chem. Phys., 5, 715–737, 2005, http://www.atmos-chem-phys.net/5/715/2005/. 3721

Lohmann, U. and Kärcher, B.: First interactive simulations of cirrus clouds formed by homogeneous freezing in the ECHAM GCM, J. Geophys. Res., 107, 4105, doi:10.1029/2001JD000767, 2002. 3726, 3743

Lohmann, U. and Roeckner, E.: The influence of cirrus cloud-radiative forcing on climate and climate sensitivity in a general circulation model, J. Geophys. Res., 100, 16 305–16 323, 1995. 3727

Lohmann, U. and Roeckner, E.: Design and performance of a new cloud microphysics scheme developed for the ECHAM general circulation model, Clim. Dyn., 12, 557–572, 1996. 3723

Lohmann, U., Feichter, J., Chuang, C. C., and Penner, J. E.: Predicting the number of cloud droplets in the ECHAM GCM, J. Geophys. Res., 104, 9169–9198, 1999. 3723, 3724, 3725

Mlawer, E. J., Taubman, S. J., Brown, P. D., Iacono, M. J., and Clough, S. A.: Radiative transfer for inhomogeneous atmospheres: RRTM, a validated correlated-k model for the longwave, J. Geophys. Res., 102, 16 663–16 682, 1997. 3723

Ou, S.-C. and Liou, K.-N.: Ice microphysics and climatic temperature feedback, Atmos. Res., 35, 127–138, 1995. 3726

Peng, Y. and Lohmann, U.: Sensitivity study of the spectral dispersion of the cloud droplet size distribution on the indirect aerosol effect, Geophys. Res. Lett., 30, 1507, doi:10.1029/2003GL017192, 2003. 3727

Roeckner, E., Arpe, K., Bengtsson, L., Christoph, M., Claussen, M., Dümenil, L., Esch, M., Giorgetta, M., Schlese, U., and Schulzweida, U.: The atmospheric general circulation model ECHAM4: Model description and simulation of the present day climate, Tech. Rep., 218, Max–Planck–Inst. für Meteorol., Hamburg, Germany, 1996. 3723

Roeckner, E., Bäuml, G., Bonaventura, L., Brokopf, R., Esch, M., Giorgetta, M., Hagemann, S., Kirchner, I., Kornblueh, L., Manzini, E., Rhodin, A., Schlese, U., Schulzweida, U., and

Tompkins, A.: The atmospheric general circulation model ECHAM5. PART I: Model description, Tech. Rep. 349, Max-Planck-Inst. für Meteorol., Hamburg, Germany, 2003. 3723, 3731, 3743

Rogers, R. R. and Yau, M. K.: A Short Course in Cloud Physics, Pergamon, Tarrytown, N. Y., 1989. 3724

Rossow, W. B. and Schiffer, R. A.: Advances in understanding clouds from ISCCP, Bull. Am. Meteorol. Soc., 80, 2261–2287, 1999. 3729, 3730, 3752

Schulz, M., Textor, C., Kinne, S., Balkanski, Y., Bauer, S., Berntsen, T., Berglen, T., Boucher, O., Dentener, F., Guibert, S., Isaksen, I. S. A., Iversen, T., Koch, D., Kirkevag, A., Liu, X., Montanaro, V., Myhre, G., Penner, J. E., Pitari, G., Reddy, S., Seland, O., Stier, P., and Takemura, T.: Radiative forcing by aerosols as derived from the AeroCom present-day and pre-industrial simulations, Atmos. Chem. Phys., 6, 5225–5246, 2006, http://www.atmos-chem-phys.net/6/5225/2006/. 3721, 3739

Schwarz, J. P., Gao, R. S., Fahey, D. W., Thomson, D. S., Watts, L. A., Wilson, J. C., Reeves, J. M., Darbeheshti, M., Baumgardner, D. G., Kok, G. L., Chung, S. H., Schulz, M., Hendricks, J., Lauer, A., Karcher, B., Slowik, J. G., Rosenlof, K. H., Thompson, T. L., Langford, A. O., Loewenstein, M., and Aikin, K. C.: Single-particle measurements of midlatitude black carbon and light-scattering aerosols from the boundary layer to the lower stratosphere, J. Geophys. Res., 111, D16207, doi:10.1029/2006JD007076, 2006. 3735, 3756

Scott, N. A., Chedin, A., Armante, R., Francis, J., Stubenrauch, C., Chaboureau, J. P., Chevallier, F., Claud, C., and Cheruy, F.: Characteristics of the TOVS Pathfinder Path-B dataset, Bull. Am. Meteorol. Soc., 80, 2679–2701, 1999. 3730, 3752

Stier, P., Feichter, J., Kinne, S., Kloster, S., Vignati, E., Wilson, J., Ganzeveld, L., Tegen, I., Werner, M., Balkanski, Y., Schulz, M., Boucher, O., Minikin, A., and Petzold, A.: The aerosol-climate model ECHAM5-HAM, Atmos. Chem. Phys., 5, 1125–1156, 2005. 3722, 3723, 3725, 3730, 3734

Stier, P., Feichter, J., Kloster, S., Vignati, E., and Wilson, J.: Emission-induced nonlinearities in the global aerosol system - results from the ECHAM5-HAM aerosol-climate model, J. Climate, 19, 3845–3862, 2006. 3743

Sundqvist, H., Berge, E., and Kristiansson, J. E.: Condensation and Cloud Parameterization Studies with a Mesoscale Numerical Weather Prediction Model, Mon. Wea. Rev., 117, 1641–1657, 1989. 3725, 3739, 3744, 3751

Susskind, J., Piraino, P., Rokke, L., Iredell, T., and Mehta, A.: Characteristics of the TOVS

Pathfinder Path A dataset, Bull. Amer. Meteorol. Soc., 78, 1449–1472, 1997. 3730, 3752
Tompkins, A. M.: A prognostic parameterization for the subgrid-scale variability of water vapor and clouds in large-scale models and its use to diagnose cloud cover, J. Atmos. Sci., 59, 1917–1942, 2002. 3725, 3739, 3743, 3744, 3745, 3751
Tompkins, A. M., Gierens, K., and Rädel, G.: Ice supersaturation in the ECMWF Integrated Forecast System, Q. J. R. Meteorol. Soc., 133, in press, 2007. 3745
Twomey, S. A.: The influence of pollution on the shortwave albedo of clouds, J. Atmos. Sci., 34, 1149–1152, 1977. 3721
Weng, F. and Grody, N. C.: Retrieval of cloud liquid water using the special sensor microwave imager (SSM/I), J. Geophys. Res., 99, 25 535–25 551, 1994. 3752
Wild, M. and Roeckner, E.: Radiative fluxes in the ECHAM5 general circulation model, J. Climate, 19, 3792–3809, 2006. 3732
Xu, K.-M. and Randall, D. A.: A Semiempirical cloudiness parameterizations for use in climate models, J. Atmos. Sci., 53, 3084–3102, 1996. 3739

**Table 1.** Sensitivity simulations.

| Simulation | Description |
|---|---|
| ECHAM5-RH | Simulation with ECHAM5-HAM with the double-moment cloud microphysics scheme using the Sundqvist et al. (1989) cloud cover parameterization that only depends on relative humidity |
| ECHAM5-COV | As ECHAM5-RH, but using the Tompkins (2002) cloud cover parameterization |
| ECHAM5-REF | Reference simulation with the standard cloud physics scheme, that only predicts the cloud water and cloud ice mixing ratios but not their number concentrations, coupled to ECHAM5-HAM and using the Sundqvist et al. (1989) cloud cover parameterization |
| ECHAM5-1985 | As ECHAM5-RH, but using the aerosol emissions that were used in ECHAM4 |
| ECHAM4 | Simulation with ECHAM4 (Lohmann and Diehl, 2006) |

**Table 2.** Annual global mean cloud and aerosol properties and TOA energy budget budget. Aerosol optical depth (AOD) is obtained from different observations (Kinne, 2007[1]). The liquid water path (LWP) observations stem from SSM/I (Ferraro et al., 1996; Greenwald et al., 1993; Weng and Grody, 1994), ISCCP and MODIS and are restricted to oceans. The values of total water path (TWP) stem from MODIS and ISCCP satellite retrievals and of water vapor mass (WVM) from MODIS. The TWP and ice water path (IWP) global means include data from land and oceans. $N_d$ and $N_i$ refer to the vertically integrated cloud droplet and ice crystal number concentration, and $r_{\mathrm{eff}}$ refers to the cloud top effective radius. Observations of $N_d$ and $r_{\mathrm{eff}}$ are obtained from ISCCP (Han et al., 1998, 1994) and are limited to 50° N to 50° S. Total precipitation ($P_{\mathrm{tot}}$) is taken from the Global Precipitation Data Set; total cloud cover (TCC) is obtained from surface observations (Hahn et al., 1994), the International Satellite Cloud Climatology Project (ISCCP) (Rossow and Schiffer, 1999) and MODIS data (King et al., 2003). The shortwave (SCF) and longwave cloud forcing (LCF) estimates are taken from Kiehl and Trenberth (1997). In addition estimates of LCF from TOVS retrievals (Susskind et al., 1997; Scott et al., 1999) are included. $r_{\mathrm{eff}}$ was not diagnosed in ECHAM4 and no estimates of $N_d$ and $N_i$ are available from ECHAM5-REF.

| Simulation | ECHAM5 –RH | ECHAM5 –COV | ECHAM5 –REF | ECHAM5 –1985 | ECHAM4 | OBS |
|---|---|---|---|---|---|---|
| LWP, $\mathrm{g\,m^{-2}}$ | 62.7 | 67.9 | 57.2 | 66.1 | 80.6 | 50-84 |
| IWP, $\mathrm{g\,m^{-2}}$ | 27.7 | 23.3 | 19.7 | 27.7 | 8.1 | |
| TWP, $\mathrm{g\,m^{-2}}$ | 83.8 | 93.7 | 77.1 | 91.3 | 82.7 | 64-155 |
| $N_d$, $10^{10}\,\mathrm{m^{-2}}$ | 4.0 | 5.0 | | 6.9 | 19.7 | 4 |
| $N_i$, $10^{10}\,\mathrm{m^{-2}}$ | 1.0 | 1.4 | | 1.2 | 0.1 | |
| $r_{\mathrm{eff}}$, $\mu$m | 10.5 | 10.1 | | 10.4 | | 11.4 |
| WVM, $\mathrm{kg\,m^{-2}}$ | 25.8 | 25.5 | 25.5 | 25.7 | 26.3 | 25.1 |
| TCC, % | 62.5 | 61.7 | 63.6 | 63.0 | 67.6 | 62–67 |
| $P_{\mathrm{tot}}$, $\mathrm{mm\,d^{-1}}$ | 2.92 | 2.94 | 2.88 | 2.90 | 2.65 | 2.74 |
| $P_{\mathrm{strat}}$, $\mathrm{mm\,d^{-1}}$ | 1.07 | 1.15 | 1.05 | 1.05 | 1.2 | |
| $P_{\mathrm{conv}}$, $\mathrm{mm\,d^{-1}}$ | 1.86 | 1.79 | 1.82 | 1.85 | 1.45 | |
| SCF, $\mathrm{W\,m^{-2}}$ | –51.3 | –48.5 | –55.5 | –52.6 | –46.4 | –50 |
| LCF, $\mathrm{W\,m^{-2}}$ | 28.2 | 26.6 | 29.5 | 28.2 | 30.8 | 22–30 |
| AOD | 0.173 | 0.165 | 0.164 | 0.173 | 0.06 | 0.15–0.19 |

**Table 3.** Annual global mean changes in aerosol optical depth, the TOA radiative budget and hydrological cycle from 1750 to present-day. Note that liquid water path changes here refer to the average over land and ocean.

| Simulation | ECHAM5 –RH | ECHAM5 COV | ECHAM5 –1985 | ECHAM4 |
|---|---|---|---|---|
| Aerosol optical depth | 0.04 | 0.042 | 0.035 | 0.04 |
| Liquid water path, $g\,m^{-2}$ | 6.5 | 9.2 | 13.6 | 12.7 |
| Ice water path, $g\,m^{-2}$ | 0.18 | 0.18 | 0.30 | 0.10 |
| $N_d$, $10^{10}\,m^{-2}$ | 1.0 | 1.4 | 3.6 | 4.1 |
| $N_i$, $10^{10}\,m^{-2}$ | 0.06 | 0.04 | 0.13 | 0.03 |
| Total cloud cover, % | 0.5 | 1.0 | 1.0 | 0.1 |
| Total precipitation, $mm\,d^{-1}$ | –0.004 | –0.011 | –0.022 | –0.052 |
| Shortwave radiation, $W\,m^{-2}$ | –2.0 | –3.2 | –3.1 | –1.8 |
| Longwave radiation, $W\,m^{-2}$ | 0.2 | 0.3 | 0.4 | 0.7 |
| Net radiation, $W\,m^{-2}$ | –1.8 | -2.9 | –2.8 | –1.0 |



ACPD
7, 3719–3761, 2007



EGU

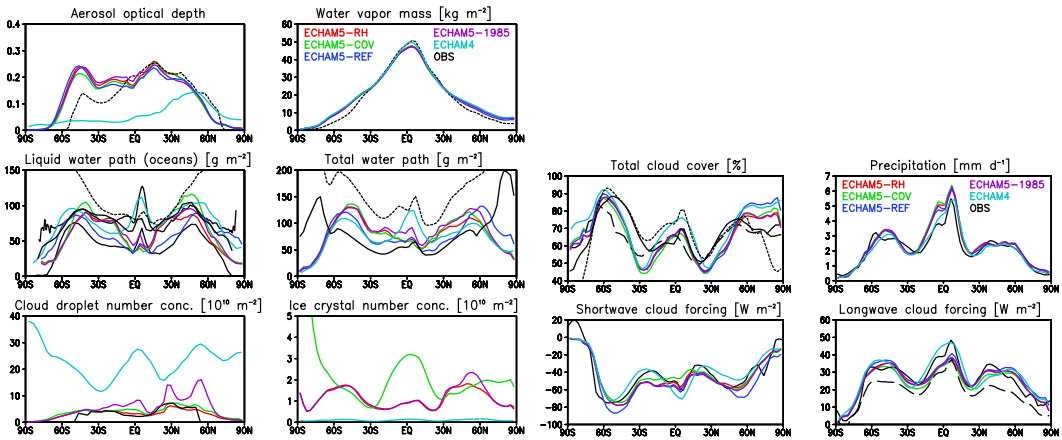


**Fig. 1.** Annual zonal means of the oceanic liquid water path (LWP), total water path, total cloud cover, total precipitation, shortwave and longwave cloud forcing, aerosol optical depth, water vapor mass, vertically integrated cloud droplet number concentration and ice crystal number concentration from different model simulations described in Table 1 and from observations described in Table 2. Solid black lines refer to SSM/I data for LWP, to ISCCP data for cloud cover and cloud droplet number concentration, and to ERBE data for cloud forcing. Dashed lines refer to surface observations for total cloud cover and to TOVS data for LCF. Dotted lines always refer to MODIS data. MODIS data of LWP and TWP are restricted to between 50° N and 50° S where they are most reliable. For AOD the combined MODIS-MISR retrieval is shown.

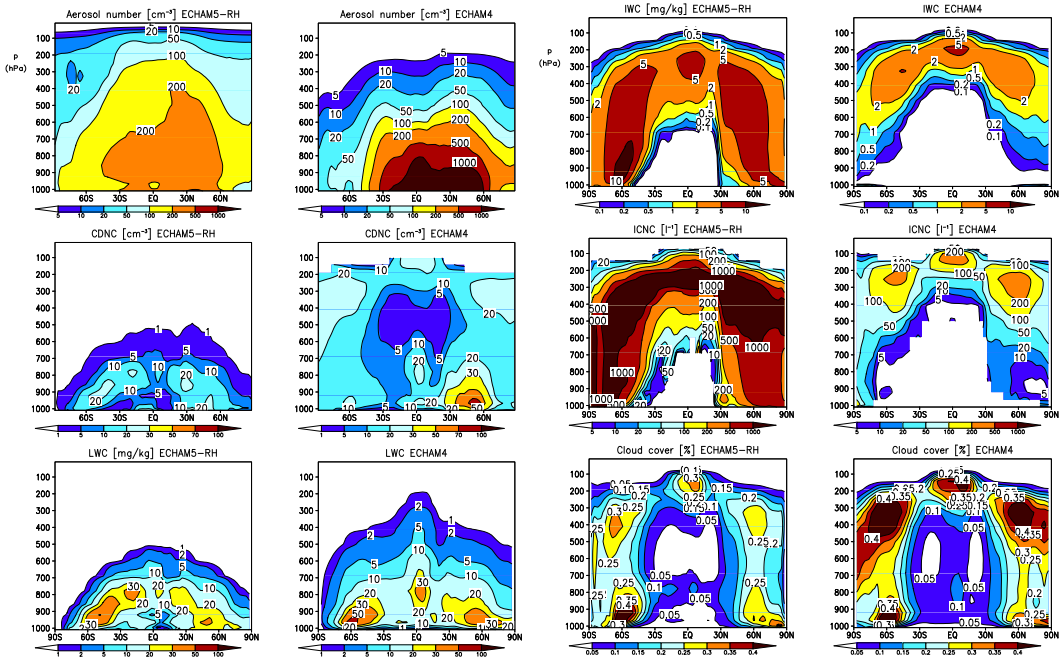


**Fig. 2.** Annual zonal mean latitude versus pressure plots of the aerosol number concentration >0.035 $\mu$m, the cloud droplet number concentration (CDNC), the liquid water (LWC) and ice water content (IWC), ice crystal number concentration (ICNC), and cloud cover from the simulation ECHAM5-RH and from ECHAM4. LWC, CDNC, IWC and ICNC are averaged over the cloudy and clear part of the grid box and are sampled over clear and cloudy periods.

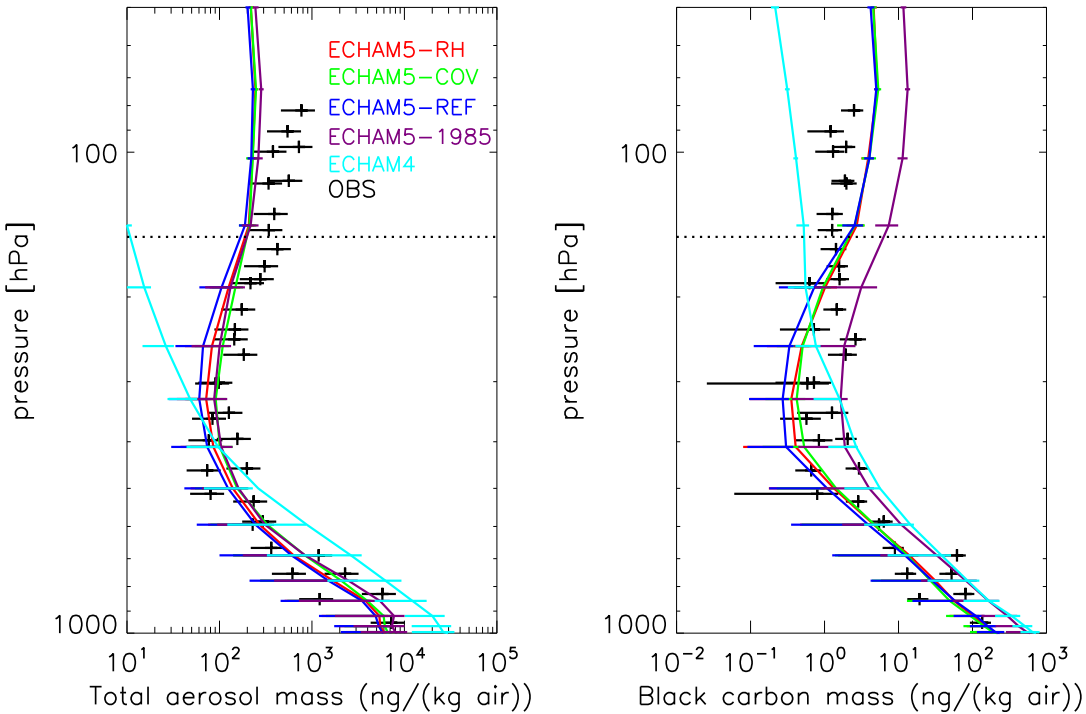


**Fig. 3.** Vertical profiles of the observed total aerosol mass plus error bars and the black carbon mass as obtained from flights out of Houston, Texas (Schwarz et al., 2006) in November 2004. The model results are shown as multi-year November averages for the geographic region between 29–38° N and 88–98° W that encompasses the aircraft flights. The model variability is identified with the 25% and 75% percentiles calculated from all 12-hourly mean concentrations obtained from the multi-year Novembers.

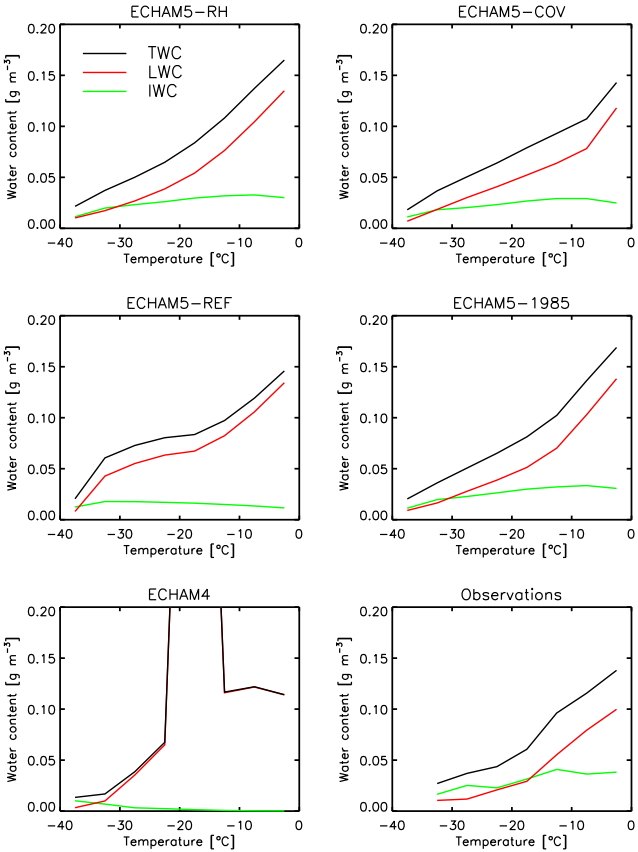


**Fig. 4.** In-cloud values of the liquid water content (LWC), ice water content (IWC) and the sum of both, the total water content (TWC), as a function of temperature from different model simulations as compared to observations from Korolev et al. (2003).

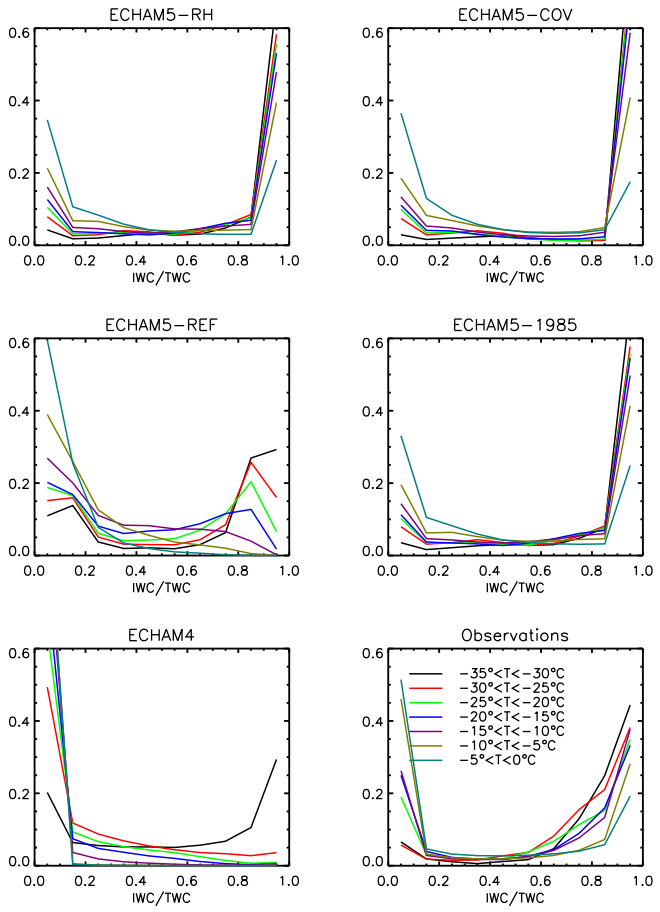


**Fig. 5.** Probability distributions of mixed-phase cloud composition (IWC/TWC) for different temperature intervals from different model simulations as compared to observations from Korolev et al. (2003).

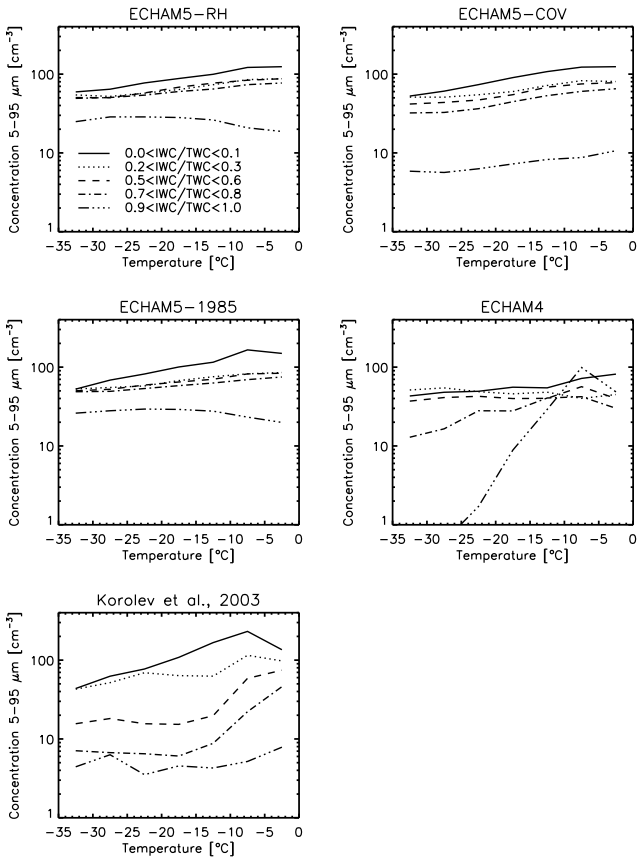


**Fig. 6.** In-cloud values of hydrometeor number concentration with diameters between 5–95 $\mu$m for different ratios of IWC to TWC. The observations stem from the forward scattering spectrometer probe (FSSP) that traditionally measures cloud droplets, but has also been used to measure ice crystal number concentrations, even though it has some caveats (Korolev et al., 2003).



ACPD
7, 3719–3761, 2007



EGU

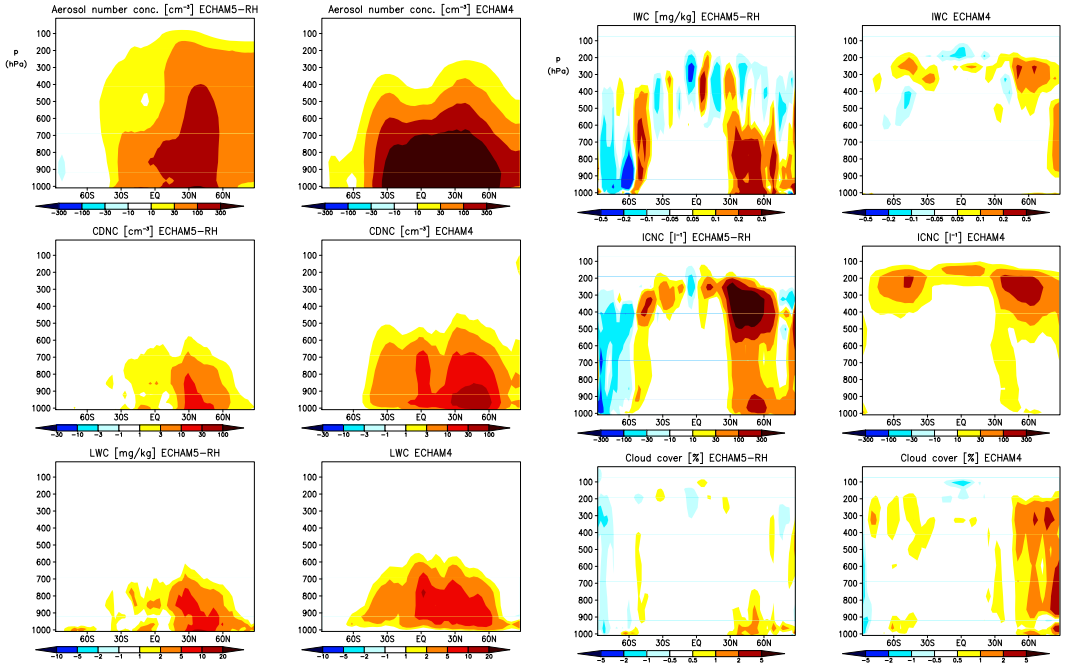


**Fig. 7.** Annual zonal mean latitude versus pressure differences of the aerosol number concentration >0.035 $\mu$m, the grid-average cloud droplet and ice crystal number concentrations (CDNC, ICNC) and mass mixing ratios (LWC, IWC) and cloud cover between present-day and pre-industrial times from ECHAM5-RH and from ECHAM4.

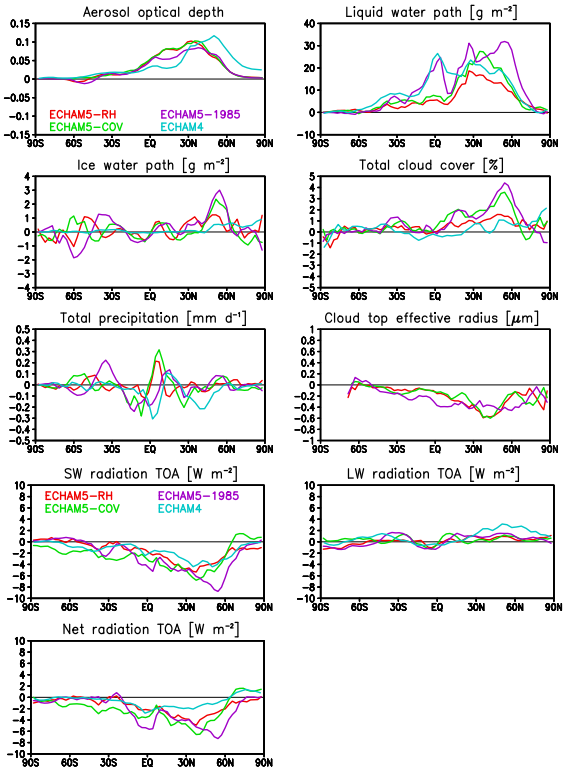


**Fig. 8.** Anthropogenic annual zonal mean differences of the aerosol optical depth, liquid water path, ice water path, total cloud cover, precipitation, shortwave, longwave net radiation at the top-of-the-atmosphere and the cloud top effective radius from the model simulations described in Table 1. Outgoing fluxes have negative signs in ECHAM, thus a positive value denotes less outgoing longwave radiation. Note that the cloud top effective radius is only sampled over cloudy periods within the cloudy part of the grid box whereas all other quantities are grid-box averages and averaged over cloudy and clear periods. Its diagnostic is not available from ECHAM4.